Chemical Science

EDGE ARTICLE

View Article Online
View Journal | View Issue

Cite this: *Chem. Sci.*, 2018, **9**, 3844

Stabilising fleeting intermediates of stilbene photocyclization with amino-borane functionalisation: the rare isolation of persistent dihydrophenanthrenes and their [1,5] H-shift isomers†

Yong-gang Shi,‡[a] Soren K. Mellerup,‡[b] Kang Yuan,[b] Guo-Fei Hu,[a] Francoise Sauriol,[b] Tai Peng,[a] Nan Wang,*[a] Pangkuan Chen*[a] and Suning Wang *[ab]

The key intermediate, 4a,4b-dihydrophenanthrene (DPH), involved in the photocyclization of stilbene and derivatives is known to be unstable, and is therefore poorly characterized/understood. We have found that functionalising stilbenes with NMe_2 and $BMes_2$ groups can greatly enhance the stability of 4a,4b-DPHs, allowing quantitative isolation and full characterization of these rare species. Furthermore, we discovered that the new amino-borane decorated 4a,4b-DPHs can undergo thermal [1,5] H sigmatropic shift, forming isomers 4a,10a-DPHs. Both 4a,4b-DHPs and 4a,10a-DHPs are stable towards air and moisture, while only the former were found to undergo oxidative dehydrogenation upon irradiation at 365 nm under air, yielding brightly blue/green fluorescent NMe_2 and $BMes_2$ functionalised phenanthrene analogues. Control studies established that the *trans*-Mes_2B–Ph–NMe_2 unit is responsible for the stability of these isolated 4a,4b-DHPs and their [1,5]-H shift isomers.

Received 2nd February 2018
Accepted 26th March 2018

DOI: 10.1039/c8sc00560e

rsc.li/chemical-science

Introduction

The field of organic photochemistry consists of many interesting and unique chemical transformations mediated by the absorption and dissipation of light. Of the many well-studied reactivities within this realm of chemistry,[1] the photocyclization of stilbene and its analogues is a prominent one.[2] These reactions proceed *via* electrocyclic ring-closure of the *cis*-isomer (*Z*) according to the Woodward–Hoffman rules[3] to give *trans*-4a,4b-dihydropheanthrene derivatives (4a,4b-DHPs, Scheme 1), which are highly unstable and either revert back to their *cis*-stilbene form or readily oxidize to their respective phenanthrenes.[4] Photochemical cyclization of stilbenes and derivatives is therefore a straightforward strategy for preparing highly diverse phenanthrenes. Despite the critical role of 4a,4b-DHPs in the formation of their phenanthrene products, little is known of the nature of these photochemically generated intermediates due to their short lifetime/poor stability. As a result, isolated and well-characterized DPHs are extremely rare and seldom observed.[5,6] In fact, nearly all of the previously known DHPs could not be isolated or obtained as pure substances due to competing side reactions and/or their poor stability toward ambient conditions.

We have discovered recently that a photoswitchable olefin system (*e.g.* *E* in Scheme 1) containing a donor–acceptor (D–A; Mes_2B–*p*-Ph–NMe_2) unit can produce the rare 4a,4b-DHP

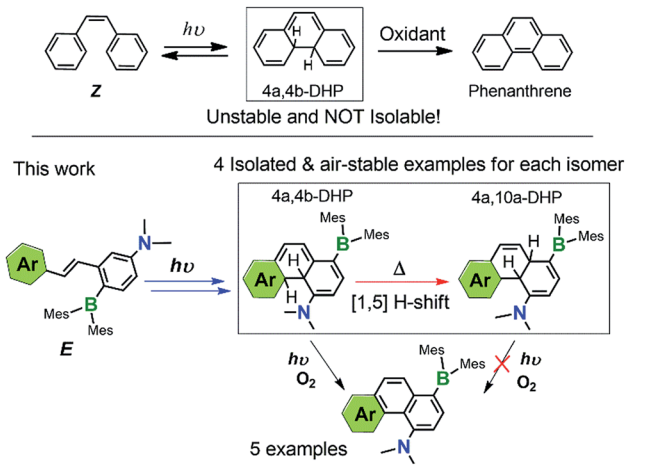

Scheme 1 Key species involved in stilbene photocyclization and donor–acceptor derivatives investigated in this work.

[a]*Beijing Key Laboratory of Photoelectronic/Electrophotonic Conversion Materials, School of Chemistry, Beijing Institute of Technology, Beijing 100081, P. R. China*

[b]*Department of Chemistry, Queen's University, Kingston, Ontario K7L 3N6, Canada. E-mail: sw17@queensu.ca*

† Electronic supplementary information (ESI) available. CCDC 1590110, 1590111, 1590113, 1816881, 1590195, 1590116, 1816882, 1590114, 1590115, 1590112, 1590109 and 1811865. For ESI and crystallographic data in CIF or other electronic format see DOI: 10.1039/c8sc00560e

‡ These authors have equal contributions to the work reported herein.

species *via* the *Z* isomer quantitatively upon irradiation, which can be isolated and are stable for days under air at ambient temperature. Furthermore, we observed that the amino-borane decorated 4a,4b-DHPs can undergo a thermal [1,5] sigmatropic H migration, forming the previously unknown 4a,10a-DHP isomers quantitatively, which are also air stable and do not dehydrogenate to the phenanthrene derivatives under any conditions. Under aerobic, photolytic conditions, the new 4a,4b-DHPs convert to phenanthrene derivatives in 40% yield, comparable to previously reported photochemical generation of phenanthrene and derivatives from stilbenes and analogues.[7] The remarkably high and unprecedented stability of the new DHPs is very unusual. The results of our study show that the stability of DHPs bearing *para*-substituted D–A systems is a general phenomenon, with varying aryl substituents exhibiting similar photoreactivity. Alterations to the D–A system (*i.e.* removal of the donor/acceptor or differing connectivity patterns) resulted in molecules that only display *trans–cis* isomerisation with irradiation. This role of the amino-borane[8] functionalities represents a new facet of such D–A systems, broadening their utility in chemical syntheses and materials applications. The details of our investigation and several mechanistic aspects of the new donor–acceptor appended photocyclization systems are presented herein.

Results and discussion

Syntheses and structures of 1a–9a

The $BMes_2$ and/or NMe_2 appended stilbene analogues **1a–9a** were prepared in high yields according to the procedures shown in Scheme 2. The ylide reagents were synthesized according to the relevant literature.[9–13] **BO-1** was prepared according to a procedure we developed recently.[14] **BO1′** and **BO1m** were prepared according to procedures outlined in the ESI.† All compounds were fully characterized by ^1H, ^{13}C and ^{11}B NMR, HRMS spectroscopic analysis. The ^{11}B chemical shifts of these compounds are between ~70–75 ppm, typical of triarylboranes.[15] Additionally, with the exception of **2a** and **8a**, the structures of these compounds were all determined by single-crystal X-ray diffraction (Fig. 1 and ESI†). All nine compounds have a *trans*-structure with respect to the olefin bond that is persistent in solution unless irradiated by UV light. The two possible *trans*-rotamers, a and b are shown in Scheme 2. In the crystal lattice, these compounds adopt the *trans*-rotamer-a structure exclusively, attributable to the reduced steric interactions between the $BMes_2$ group and the olefin unit in this conformation. The crystal structures of ***E*-1a** and ***E*-9a** are shown in Fig. 1 as representative examples (see ESI† for the others). The NMe_2 group in these molecules is coplanar with the phenyl ring. One important feature of the D–A-functionalised stilbene ***E*-1a** is that the benzene ring containing the donor and acceptor groups has a quinoid-like structure caused by the push–pull substituents.[21b,d] Similar C–C bond length variations in the benzene ring of the D–A system were found for ***E*-3a**, ***E*-4a**, ***E*-6a** and ***E*-7a**, which agree well with those calculated by DFT for the parent molecule Mes_2B–Ph–*p*-NMe_2 (see ESI†). As a consequence of the quinoid-like structure, the Mes_2B–Ph–*p*-NMe_2

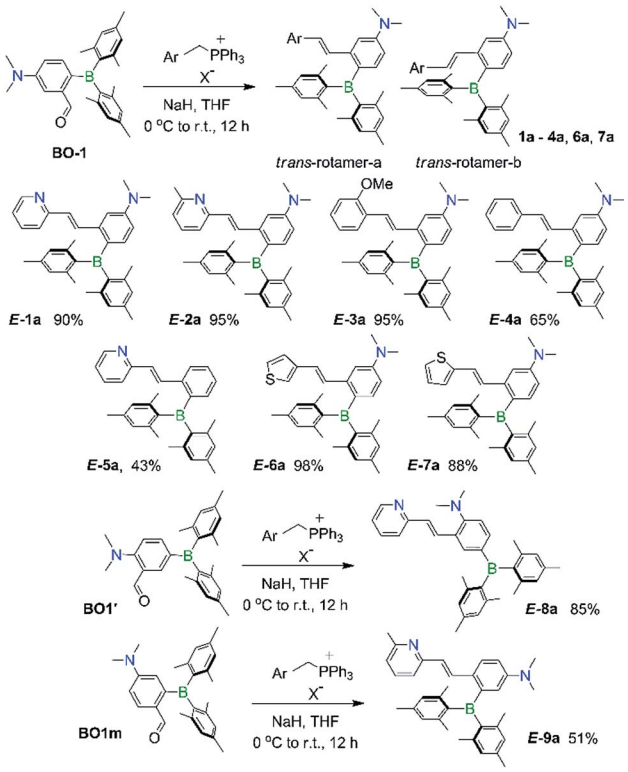

Scheme 2 The synthetic routes of compounds *E*-1a–*E*-9a investigated in this work.

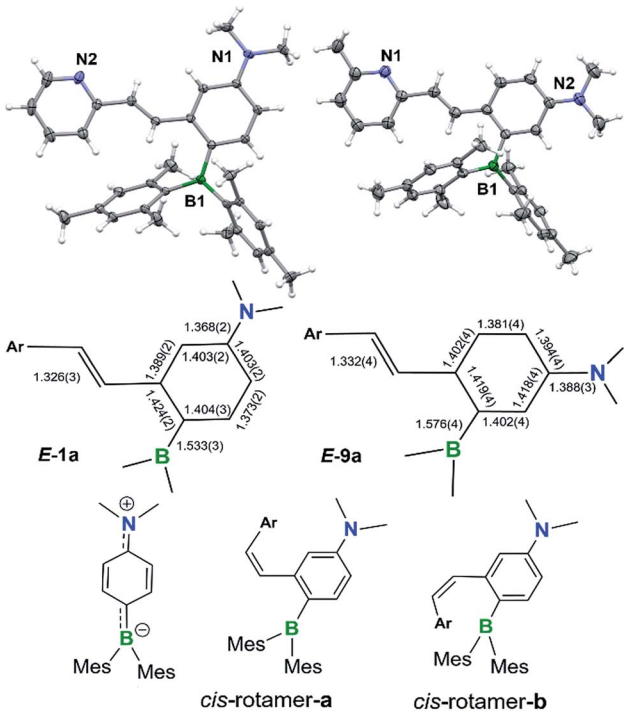

Fig. 1 Top: crystal structures of *E*-1a (left) and *E*-9a (right) with 35% thermal ellipsoids with the key bond lengths (Å) shown in the schematic representation of their structures. Bottom: the structures of the *cis*-rotamers and the quinoid resonance form of the *para*-substituted D–A unit.

ring has a lower aromaticity compared to that of benzene as evidenced by the NICS values calculated by DFT: NICS(0) and NICS(1) for Mes_2B–Ph–*p*-NMe_2 are −7.58 and −9.36, respectively, while those for benzene are −9.86 and −11.20, respectively. These bonding features are in contrast to the structure of ***E*-9a**, where *meta*-substitution of the D–A system across the phenyl ring yields bond lengths more similar to those of benzene (Fig. 1).

The *cis*-isomers of compounds **1a–9a** also have two possible rotamers a and b shown in Fig. 1 with the *cis*-rotamer-a being favoured due to its reduced steric congestion compared to *cis*-rotamer-b. DFT computational data indicate that *cis*-rotamer-a is ∼3–5 kcal mol^{-1} higher in energy than that of the respective *trans*-rotamer-a for **1a–9a**.

Photoreactivity of *E*-1a–*E*-9a and the isolation of DHPs 1b–4b

Compounds ***E*-1a–*E*-4a** and ***E*-6a–*E*-8a** have a light-yellow colour with intense absorption bands at λ_{max} = ∼360–380 nm (ε = ∼17000 to 28000 M^{-1} cm^{-1}) in THF. They are all brightly fluorescent, emitting a sky-blue colour (λ_{em} = ∼460–480 nm) in THF under UV light, with Φ_{FL} = 0.26 to 0.41 (see Table 1). TD-DFT computational data shows that the $S_0 \rightarrow S_1$ transition for these molecules primarily involves HOMO and LUMO orbitals (∼90%) with a large oscillator strength. The HOMO is located mainly on the NMe_2-phenyl portion while the LUMO spreads over the entire molecule with a large contribution from the boron atom. In contrast, the acceptor-only molecule ***E*-5a** is colourless with an absorption band at λ_{max} = ∼300 nm, and is weakly blue emissive (λ_{em} = 450 nm, Φ_{FL} = 0.06 in THF). The *meta*-D–A substituted molecule ***E*-9a** has a significantly red shifted absorption and emission band with a greater emission efficiency (λ_{em} = 536 nm, Φ_{FL} = 0.65), compared to those of ***E*-1a–*E*-8a** (see Table 1 and ESI†).

Table 1 Absorption and fluorescence data of the isolated compounds reported in this work

Compound	Absorption in THF λ_{abs} (nm) (ε, M^{-1} cm^{-1})	Fluorescence in THF λ_{em} (nm)	Φ_{FL}[a]
***E*-1a**	315 (35457), 384 (19155)	483	0.39
1b	414 (21282)	464	0.03
1c	422 (24494)	435	0.06
1d	305 (16521), 374 (16133)	480	0.49
***E*-2a**	318 (32368), 382 (17130)	484	0.40
2b	415 (22839)	462	0.01
2c	422 (28856)	471	0.03
2d	306 (17036), 375 (15802)	480	0.54
***E*-3a**	321 (27864), 379 (22173)	476	0.41
3b	418 (24133)	469	0.01
3c	424 (29914)	468	0.03
3d	314 (20179), 383 (15967)	480	0.41
***E*-4a**	315 (37129), 382 (22122)	478	0.43
4b	417 (22283)	434	0.01
4c	423 (27366)	472	0.02
4d	313 (17469), 378 (14129)	480	0.49
***E*-5a**	304(27602)	450	0.06
***E*-6a**	315 (39642), 380 (27831)	473	0.37
6d	272 (19697), 294 (15720), 374 (13113)	480	0.45
***E*-7a**	325 (34151), 380 (21960)	485	0.26
***E*-8a**	318 (42807), 357 (32632)	463	0.38
***E*-9a**	333 (18568), 362 (18454), 420 (6833)	536	0.65

[a] Determined with an absolute QY spectrometer.

Despite their highly emissive nature (excluding ***E*-5a**) and congested structures, ***E*-1a–*E*-9a** all undergo photoisomerisation upon irradiation at 365 nm under nitrogen in benzene or THF, which were monitored by NMR, UV-vis and fluorescence spectroscopy. The photoreactions of ***E*-1a–*E*-4a** are similar while those of ***E*-5a–*E*-9a** are quite different. The discussion will focus on the phototransformation of compounds ***E*-1a–*E*-4a** first, using ***E*-2a** as a representative example. As shown by the time-lapsed ^{1}H NMR spectra of ***E*-2a** (1 mg of ***E*-1a** in 0.6 mL of C_6D_6, Fig. 2), within minutes of irradiation at 365 nm, ***Z*-2a** (*cis*-rotamer-a) forms and becomes the dominating species. The ^3J olefin proton coupling constant decreases from 16.0 Hz in ***E*-2a** to 12.4 Hz in ***Z*-2a**, which agrees with previous reports in the literature.[16] In addition, a new set of peaks that were assigned to the DHP **2b** also begin to appear in the spectrum. After about 2 hours of irradiation, ***E*-2a** and ***Z*-2a** are fully and cleanly converted to the bright yellow compound **2b**. The characteristic NMR features of **2b** are the two peaks at 3.87 and 3.68 ppm, respectively, which have a typical AB splitting pattern with a ^3J coupling constant of 20.7 Hz. 2D-NOESY NMR experiments established that these two H atoms are arranged in a *trans*-configuration with respect to one another (H_a and H_b, Fig. 2; see also Fig. S6 in the ESI†). H_a is further coupled to the adjacent H_c (^3J = 4.7 Hz) and H_d (^5J = 2.5 Hz) atoms. The formation of a *trans*-4a,4b-DHP (**2b**) from the photocyclization of ***Z*-2a** is in agreement with a conrotatory electrocyclization, as predicted by the Woodward–Hoffman rules. Due to the different substituents on the alkenyl moiety, **2b** represents the very first example of a 4a,4b-DHP where coupling of the inner H atoms is directly observed. Interestingly, NMR tracking indicated that compound **2b** is air-stable for days in solution at ambient temperature and

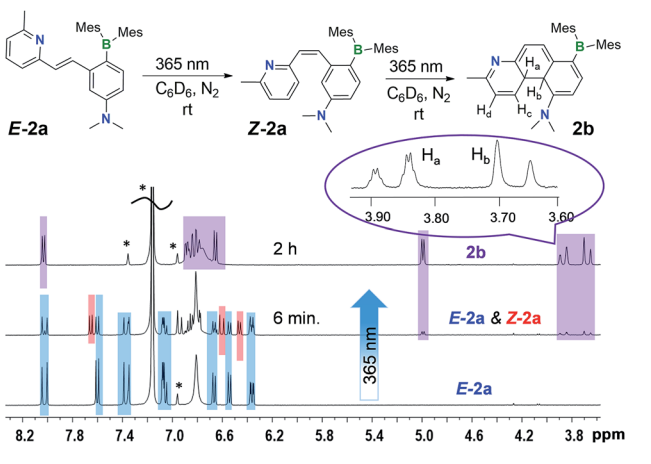

Fig. 2 ^{1}H NMR spectral change (the aliphatic region is omitted for clarity) of ***E*-2a** (1 mg in 0.6 mL of C_6D_6) with 365 nm irradiation at ambient temperature under N_2. The representative peaks for each species are colour-coded (blue: ***E*-2a**; red: ***Z*-2a**; purple: **2b**). The solvent peak and the spin sidebands are indicated by *.

does not dehydrogenate to the expected phenanthrene product (see Fig. S29 in the ESI†). As such, **2b** can be isolated and studied as a pure compound, which is exceedingly rare for 4a,4b-DHP systems. Nonetheless, efforts to obtain single-crystals of **2b** for X-ray diffraction analysis have not been successful.

The transformation of ***E*-2a** to **2b** can also be tracked by UV-vis and fluorescence spectroscopy. In the UV-vis spectra, a clear sequential spectral change was observed (Fig. 3). Irradiation first causes the absorption band of ***E*-2a** at 318 nm to decrease and a hypsochromic shift of the band at 382 nm to 368 nm is observed with clear isosbestic points. This portion of spectral change is attributed to the formation of ***Z*-2a**, which is in agreement with previously reported *trans* to *cis*-isomerisation of stilbenes and derivatives.[4] TD-DFT computational data also confirmed the hypsochromic shift (385 to 360 nm) of the first vertical excitation band from ***E*-2a** to ***Z*-2a**. The ***Z*-2a** absorption band decreases with irradiation time, accompanied by the rise of a low energy band at 415 nm, which is assigned to **2b**. In the fluorescence spectra, the emission peak of ***E*-2a** decreases sharply in intensity as it is converted to ***Z*-2a** and **2b**. Compound **2b** is weakly blue fluorescent with $\lambda_{em} = 462$ nm and $\Phi_{FL} = 0.03$. TD-DFT data indicated that the $S_0 \rightarrow S_1$ vertical excitation in **2b** is a HOMO to LUMO transition (100%) localized on the DHP unit with a high oscillator strength and little contributions from the boron unit (see ESI†).

NMR, UV-vis and fluorescence spectral tracking showed that with 365 nm irradiation, ***E*-1a**, ***E*-3a** and ***E*-4a** all undergo a similar transformation as that of ***E*-2a**, forming the corresponding DHPs **1b**, **3b** and **4b** quantitatively *via* the *cis*-stilbene intermediate (*Z*). The $^3J_{H_a-H_b}$ coupling constants (20.5–20.7 Hz) in **1b**, **3b** and **4b** are similar to that of **2b** (see ESI†). Like **2b**, compound **1b** is also stable for days in solution under ambient conditions. For **3b** and **4b**, after one day of standing under air at ambient temperature, a small amount of their [1,5] H-shifted products, **3c** and **4c**, were observed by NMR, which will be discussed in the following section. Again, **1b**, **3b** and **4b** do not undergo dehydrogenation under ambient conditions. Similar to **2b**, these three compounds are weakly fluorescent with $\lambda_{em} =$ 460–470 nm and $\Phi_{FL} = 0.01$–0.03. The photophysical data of **1b**–**4b** are summarized in Table 1.

The unusually high stability of **1b**–**4b** is not fully understood, although we postulate that the kinetic barrier for their reversal back to ***Z*-1a**–***Z*-4a** is likely very high. DFT optimized structures show H-bond interactions between the amino nitrogen atom and nearby H atoms such as the inner H_b in **1b**–**4b**, which may contribute to the stability of these DHPs. The coexistence of the $BMes_2$ and NMe_2 group in **1b**–**4b** appears to be essential for their formation and stability, as the previously reported[17] analogue of **1a** that lacks the $BMes_2$ group does not produce a stable DHP, while that which lacks the NMe_2 group (***E*-5a**) is photoreactive but does not form a DHP at all (see Fig. S19 in the ESI†). The products of ***E*-5a** phototransformation have not been determined and are beyond the scope of this current investigation. The other key factor for the stability of **1b**–**4b** is the presence of an alternative isomerisation pathway for these molecules, namely a thermal [1,5] H migration, leading to the generation of much more stable isomers **1c**–**4c** which are described in the next section.

Compound ***E*-6a** behaves similarly to compounds ***E*-1a**–***E*-4a**, but only partially converts to the cyclized compound **6b** at 365 nm, which undergoes decomposition with further irradiation. Irradiation at 410 nm converts **6b** back to ***Z*-6a**. Due to its poor stability, **6b** was not isolated. In contrast to ***E*-1a**–***E*-4a**, compounds ***E*-7a**–***E*-9a** only undergo *trans*–*cis* isomerisation upon irradiation at 365 nm, reaching their photostationary states with approximately 1 : 1 ratio of the *E vs. Z* isomers in solution, and no observable cyclization (see ESI†). In ***E*-8a**, the positions of the NMe_2 and $BMes_2$ groups are switched compared to those in ***E*-1a**. The lack of photocyclization observed for ***E*-8a** may be attributed to the steric congestion imposed by the bulky $BMes_2$ that prevents C–C bond formation at the adjacent carbon atom. In ***E*-9a**, the NMe_2 and $BMes_2$ groups are *meta* to each other, as opposed to *para* in the other derivatives. The lack of photocyclization for ***E*-9a** further confirms the necessity of the *para*-D–A system (and its resulting quinoidal structure) in the phototransformation.

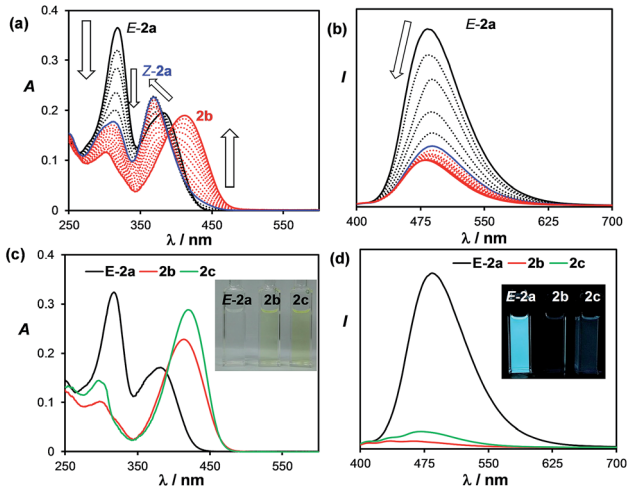

Fig. 3 Top: UV-vis (a) and fluorescence (b) spectral change of ***E*-2a** in THF upon irradiation at 365 nm (the final spectrum corresponds to ~80% formation of **2b**. Bottom: the UV-vis (c) and fluorescence (d) spectra of isolated ***E*-2a**, **2b**, and **2c** in THF (1.0×10^{-5} M). Inset: photographs showing the absorption and emission colours and relative intensity of ***E*-2a**, **2b**, and **2c** in THF.

[1,5] H migration of 1b–4b and the isolation of 4a,10a-DHPs 1c–4c

An interesting observation we made is that compounds **1b**–**4b** can undergo further structural change, producing isomers **1c**–**4c**, respectively, either after an extended period of irradiation at 365 nm or heating. Careful control of the experimental conditions indicated that this new transformation is a thermal process. Heat generated from the photo reactor during irradiation is sufficient to drive this rearrangement reaction in some of the DHPs. The thermal isomerisation of **2b** is described here as a representative example.

The ^{1}H NMR spectra in Fig. 4 show that **2b** transforms to **2c** quantitatively upon heating in a benzene solution at 120 °C for ~24 hours (1 mg in 0.6 mL of C_6D_6). The structural assignment of **2c** was accomplished first by 1D and 2D NMR spectroscopic analyses, which indicated that **2c** is an analogue of *cis*-4a,10a-DHP. The chemical shifts of the two inner H atoms, H_a and H_b, appear at 3.51 and 3.57 ppm, respectively, with a ^3J coupling constant of 7.6 Hz, much smaller than that observed in **2b**. The H_a atom is further coupled to H_c and H_d with $^3J_{H_a-H_c} \approx {}^3J_{H_a-H_b} \approx$ 7.6 Hz and $^3J_{H_a-H_d} = 2.0$ Hz. Compound **1b** undergoes a similar transformation, forming **1c** quantitatively at 120 °C, with a similar ^{1}H NMR spectral change as observed for the **2b** to **2c** conversion (see ESI†). Surprisingly, compounds **1c** and **2c** are stable under air for days, and can even be purified by column chromatography under air. The crystal structures of **1c** and **2c** were determined by single-crystal X-ray diffraction analyses, which confirmed the *cis*-4a,10a-DHP structure for both. The structure of **2c** is shown in Fig. 5 and that of **1c** is provided in the ESI.† Although various H migrations of 4a,4b-DHPs and derivatives were described previously[6,18] and implicated in some phototransformations of stilbenes, no H migrated species/intermediates have been isolated and fully characterized to date. Compounds **1c** and **2c** are therefore the first examples of structurally characterized 4a,10a-DHPs. Formally, the transformation of **1b**–**2b** to **1c**–**2c** can be described as a [1,5] H migration.

For **3b** and **4b**, heating their benzene solutions at 90 °C for a few hours can fully convert them to **3c** and **4c**, respectively, an indication that the activation barriers for the [1,5] H migration of **3b** and **4b** are lower than those of **1b** and **2b**. Again, compounds **3c** and **4c** are stable under air in solution and the solid state, with their two inner H atoms having a *cis*-geometry. Compounds **1c**–**4c** have a similar yellow colour and are weakly emissive like their **1b**–**4b** isomers. For comparison, the UV-vis and fluorescence spectra of the isolated ***E*-2a**, **2b** and **2c** in THF are shown in Fig. 3. The full spectroscopic and characterization data for **1c**–**4c** are provided in the ESI.† Heating the solution mixture of compounds ***Z*-6a** and **6b** obtained from the photolysis of ***E*-6a** only led to the reversal of **6b** back to ***Z*-6a**.

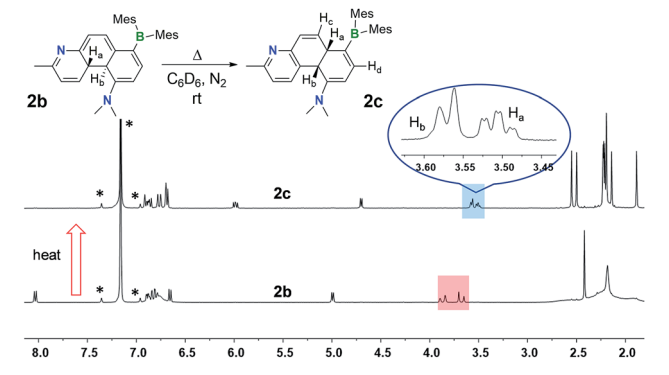

Fig. 4 ^{1}H NMR spectra showing the clean conversion of **2b** to **2c** in C_6D_6 upon heating at 120 °C for 24 hours. The solvent peak and its spin satellite peaks are indicated by *.

One thing that is curious is the *cis*-configuration of the products **1c**–**4c**, as thermal [1,5] sigmatropic shifts proceed suprafacially and the two inner H atoms should therefore have a *trans*-geometry. DFT computational analysis indicate that the *cis*-**1c** is about 10 kcal mol^{-1} more stable than *trans*-**1c** (see ESI†). To further understand the H migration process, we prepared compound ***E*-4a′** in which the phenyl ring has been deuterated (C_6D_5). Irradiation of ***E*-4a′** in C_6D_6 at 365 nm followed by heating at 110 °C led to the quantitative isolation of the *cis*-4a,10a-DHP **4c′**. Analysis and comparison of the ^{1}H NMR spectra of **4c** and **4c′** (Fig. 6) established unequivocally that the H_a atom in **4c** is completely replaced by a D atom in **4c′**, confirming that the migrated H atom is indeed from the phenyl ring and the migratory process is intramolecular. From this finding, we suspect that the *cis*-product **4c** is formed through an internal base (the amino group) promoted configuration inversion of the carbon atom that is bound to H_b. Base induced proton tautomerism in DHPs and derivatives was observed/proposed previously,[6] although no detailed spectroscopic information is available.

To examine the possible involvement of the amino group in the formation of the *cis*-product **4c**, the [1,5] H migration of **4b** was repeated in C_6D_6 (1 mg/0.6 mL of solvent) with the addition of one drop of D_2O. Heating at 120 °C for ~44 hours led to the quantitative isolation of compound **4c″** (Fig. 7). The ^{1}H NMR spectrum of **4c″** shows 100% H–D exchange of the H atom *ortho* to the NMe_2 group and ~50% H–D exchange for the H_b atom (see Fig. S18 in the ESI†). Based on these observations, a plausible mechanism for the **4b** to *cis*-**4c** conversion is shown in Fig. 8. The **4c-TS** in Fig. 8 is likely responsible for the H–D exchange with D_2O, where the H_b is in the process of being shuttled to the opposite face of the molecule by the basic N atom.

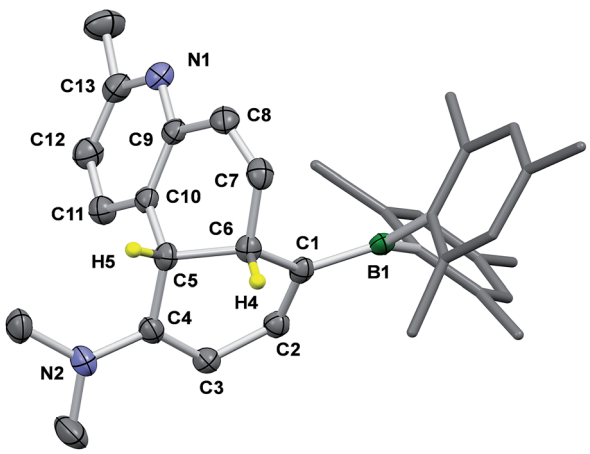

Fig. 5 The crystal structure of **2c** with the key atoms being labelled and 35% thermal ellipsoids. H atoms except the two inner ones are omitted for clarity. Selected bond lengths (Å) for **2c**: C(1)–C(2) 1.366(3), C(2)–C(3) 1.427(3), C(3)–C(4) 1.366(3), C(4)–C(5) 1.514(3), C(5)–C(6) 1.543(3), C(5)–C(10) 1.524(3), C(6)–C(7) 1.513(3), C(7)–C(8) 1.322(3), C(8)–C(9) 1.468(3), C(9)–C(10) 1.391(3), C(10)–C(11) 1.385(3), C(11)–C(12) 1.382(3), C(12)–C(13) 1.376(3), N(1)–C(9) 1.345(3), N(1)–C(13) 1.352(3), C(1)–B(1) 1.530(3), N(2)–C(4) 1.362(3).

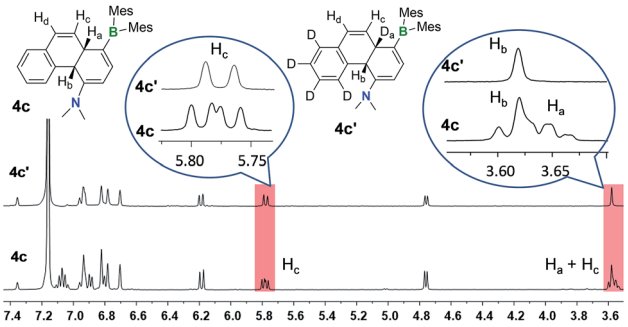

Fig. 6 ^{1}H NMR spectra of **4c** and **4c′** in C_6D_6 showing the disappearance of peaks and coupling pattern change due to D substitution in **4c′**.

The kinetics of the [1,5] sigmatropic shift were investigated for **2b**, **3b** and **4b**. The data show unambiguously that the b to c transformation follow first-order kinetics (see ESI Section S6†), consistent with a concerted intramolecular H migration.[19] Using the rate constants obtained in benzene at three different temperatures, the activation energies were determined to be 30.0(4), 25(1), and 27.9(5) kcal mol^{-1} for **2b** to **2c**, **3b** to **3c** and **4b** to **4c** conversion, respectively. The kinetics of the [1,5] H migration is therefore greatly influenced by the nature of the aryl group in **b**, with the rate constants following the order of MeO-phenyl > phenyl > 2-Me-py. The aromaticity of these aryl groups follows the same order (as calculated by DFT methods, see ESI†). This correlation is reasonable, as the transition state of [1,5] H migration (**b** to **c** conversion) involves the aryl ring re-aromatization; thus greater aromaticity likely helps to stabilize the transition state and reduce the activation barrier. DFT computational studies indicate that the energies of *cis*-**1c–4c** are about 30 to 33 kcal mol^{-1} lower than **1b–4b**. Thus, the [1,5] H migration is a thermodynamically driven process as illustrated in Fig. 8. Compounds *cis*-**1c–4c** are only about 10 kcal mol^{-1} above ***E*-1a–4a** (see Table S65† for the complete DFT data). Again, the donor and the acceptor units are believed to play a key role in the exceptionally high stability of *cis*-**1c–4c** and their inactivity toward air under ambient conditions.

Oxidative dehydrogenation of DHPs 1b–4b, 6b and the isolation of phenanthrenes 1d–4d and 6d

Although the DHPs **1b–4b** do not react with oxygen under ambient conditions, they do behave like typical DHPs and undergo photo-oxidative dehydrogenation when irradiated at

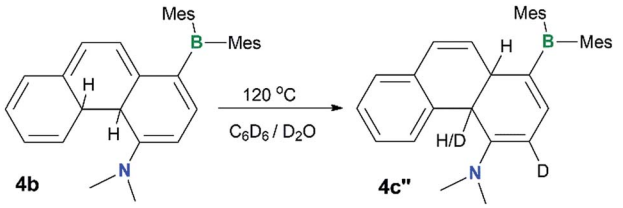

Fig. 7 A diagram showing the H–D exchange in the thermal conversion of **4b** to **4c″** in C_6D_6 in the presence of a drop of D_2O.

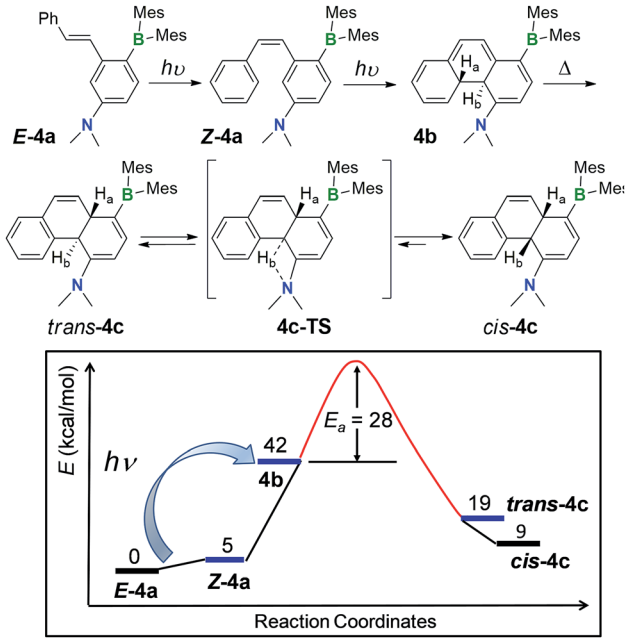

Fig. 8 Top: proposed mechanism for the transformation of ***E*-4a** to *cis*-**4c**. Bottom: relative energies of the various species involved in the transformation calculated at the M06-2X/6-31+g(d,p) level of theory, as well as the experimentally determined activation barrier for **4b** to **4c** isomerization in C_6D_6.

365 nm under air, producing the fully conjugated phenanthrene derivatives **1d–4d** in about 30–40% yields, accompanied by various decomposed and unidentifiable species. Photolysis of ***E*-1a–4a** at 365 nm under air at ambient temperature produced a similar mixture of products with 30–37% isolated yields of **1d–4d**. Although ***E*-6a** only partially converts to **6b** when irradiated under nitrogen, it converts to the aromatic compound **6d** when irradiated under air, which was isolated in 37% yield. This demonstrates that photocyclization of the simple stilbene derivative compounds ***E*-1a–4a/6a** is a viable approach for achieving the amino/boryl functionalised phenanthrene derivatives **1d–4d/6d** (Fig. 9), which would not be easy to obtain by other methods. Given the fact that the oxidative dehydrogenation reactions of stilbenes are well established and known to

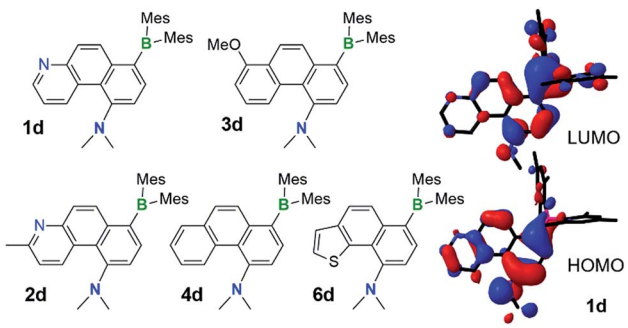

Fig. 9 The structures of isolated NMe_2 and $BMes_2$ functionalised phenanthrene derivatives **1d–4d** and **6d**, the HOMO and LUMO diagrams of **1d** (DFT at B3LYP/6-31(d) level of theory).

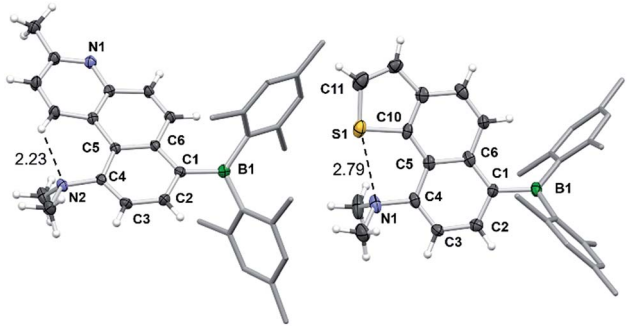

Fig. 10 The crystal structures of **2d** and **6d** with 35% thermal ellipsoids and labels for selected atoms. Selected bond lengths (Å) for **2d**/**6d**: B(1)–C(1) 1.569(4)/1.580(10), C(1)–C(2) 1.383(3)/1.389(10), C(2)–C(3) 1.386(3)/1.420(10), C(3)–C(4) 1.383(3)/1.366(10), C(4)–C(5) 1.493(3)/1.457(10), C(5)–C(6) 1.432(3)/1.460(9), C(4)–N(2)/N(1) 1.419(3)/1.441(8), S(1)–C(10) 1.743(7), S(1)–C(11) 1.722(10).

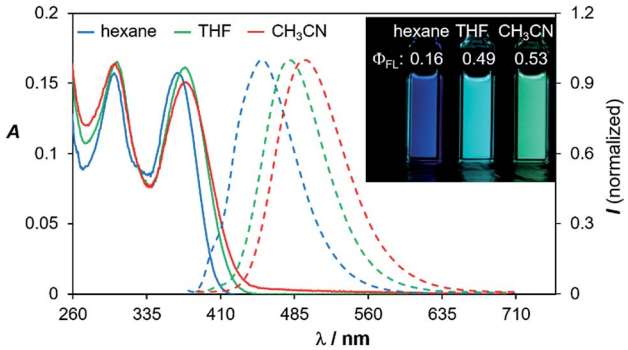

Fig. 11 Absorption and fluorescence spectra of compound **1d** in three different solvents (1×10^{-5} M). The fluorescence spectra were recorded at λ_{max} of absorption. Inset: photographs showing the emission colours and Φ_{FL} of **1d** in the three different solvents.

produce phenanthrenes in low to moderate yields when air is used as the oxidant, attempts were not made to further optimize this reaction. ***E*-8a–9a** undergo *trans* to *cis* isomerisation only when irradiated at 365 nm under air and no dehydrogenated products were observed at all, which is consistent with their inability to undergo photocyclization.

Surprisingly, the DHPs *cis*-**1c–4c** did not produce the dehydrogenated products **1d–4d** upon irradiation under air. Instead, complete decomposition affording unidentifiable products occurred. These results support that 4a,10a-DHP isomers such as *cis*-**1c–4c** are likely not involved in the formation of phenanthrenes and derivatives *via* the photocyclization of stilbenes. Compounds **1d–4d** and **6d** were fully characterized by NMR and HRMS analyses, while single-crystal X-ray diffraction analyses were performed on **1d**, **2d** and **6d**. The structures of **2d** and **6d** are shown in Fig. 10 and that of **1d** is provided in the ESI.† In all three structures the amino group is tilted towards the inner side of the three fused aryl rings, with its two methyl groups being above and below the plane of the molecule. The dihedral angle between the NCC plane of the NMe_2 and the benzene ring is ~61° for **1d** and **2d**, and of ~71° for **6d**, which is clearly necessary in order to minimize steric interactions between the methyl groups and the inner H atom in **1d** and **6d**. In addition, H-bonding between the N atom and the inner H atom (N···H = 2.26 Å, **1d**; 2.23 Å, **2d**) also favours this tilting of the amino unit. For **6d**, a short contact distance is noted (2.79(1) Å) between S and N, which is less than the sum of van der Waals radii of nitrogen and sulphur (3.39 Å). This "chalcogen bonding interaction[20]" may be responsible for the amino group tilting toward the sulfur atom in **6d**. The outer benzene ring and the py ring have a dihedral angle of 11° in **1d** and **2d**, while the thienyl ring is coplanar with the fused naphthyl ring in **6d**. No intermolecular π-stackings are observed in all three crystal lattices.

Compounds **1d–4d** and **6d** have a light-yellow colour and are brightly fluorescent with λ_{em} = ~480 nm and Φ_{FL} = 0.41–0.54 in THF. The emission spectra of **1d–4d** and **6d** show significant bathochromic shifts with increasing solvent polarity, which indicates the presence of a polarised excited state (Fig. 11).[21] TD-DFT computational results established the involvement of the NMe_2 and the $BMes_2$ group in the HOMO and LUMO levels, respectively (Fig. 9), with the vertical excitation to the first excited state primarily involving the HOMO to LUMO transition (>90%) with a very high oscillator strength for **1d–4d** and **6d** (see ESI†). Nonetheless, in addition to the amino and boryl units, the polycyclic aromatic rings have a great contribution to both HOMO and LUMO levels as shown by the Frontier orbital diagrams of **1d** in Fig. 9. One noteworthy feature of compounds **1d–4d** and **6d** is that they maintain a very high emission quantum efficiency in high polarity solvents such as CH_3CN (*e.g.* 0.53 for **1d**, 0.57 for **2d** and 0.55 for **4d**; see Fig. 11 and ESI†). This may be caused by an increased NMe_2 to $BMes_2$ charge transfer contribution to the first excited state in polar solvents, which is known to greatly enhance emission quantum efficiency of the molecule.[8,21]

Conclusions

In summary, a novel series of D–A functionalised stilbenes has been prepared and their photoreactivity established. Following *trans–cis* isomerisation induced by light, compounds **1a–4a** undergo photochemically allowed electrocyclic ring-closure to afford highly persistent and air-stable **1b–4b** which represent some of the only examples of fully characterizable *trans*-4a,4b-DHPs. Based on control experiments, the quinoidal structure imposed by the D–A system is the key to the stability of these DHPs. Upon heating, these species undergo a unique [1,5]-sigmatropic H atom migration and subsequent internal base-induced tautomerization to give *cis*-4a,10a-DHPs **1c–4c**, which represent a new class of stable DHP isomers. Importantly, we have shown that these DHP isomers do not dehydrogenate and are therefore not part of the DHP oxidation pathway. In the presence of air and light, **1b–4b** and **6b** are converted to their fully conjugated dehydrogenation products **1d–4d** and **6d**, which are brightly emissive even in high polarity solvents such as CH_3CN. The unprecedented stability of the 4a,4b- and 4a,10a-DHP isomers in this study offers rare snapshots into the individual steps involved in the conversion of stilbenes to phenanthrenes, thereby broadening our understanding of this photochemical transformation.

Experimental

General procedure

All solvents were freshly distilled over sodium metal and stored under nitrogen prior to use. All starting materials were purchased from Energy Chemical. (Pyridin-2-ylmethyl)triphenylphosphonium chloride,[9] 2-metho-xybenzyltriphenylphosphonium chloride,[10] benzylphosphonium bromide,[11] 2-thienylmethyltriphenylphosphonium chloride,[12] 3-thienylmethyltriphenylphosphonium bromide,[13] 2-dimesityl-borylbenzaldehyde,[22] 2-bromo-4-(dimethylamino)benzalde-hyde,[23] and 5-bromo-2-(dimethylamino)benzaldehyde[24] were synthesized according to procedures reported in literature. The starting materials for ***E*-8a** and ***E*-9a** (**BO1′** and **BO1m**, respectively) were prepared according to procedures outlined in the ESI.† All the reactions were performed under nitrogen and in dry solvents. ^{1}H, ^{13}C and ^{11}B NMR spectra were recorded on a 400 or 700 MHz spectrometer. ^{1}H and ^{13}C chemical shifts are reported in ppm relative to the signals corresponding to the residual non-deuterated solvents ($CDCl_3$: ^{1}H 7.26 ppm, ^{13}C 77.23 ppm; CD_2Cl_2: ^{1}H 5.32 ppm, ^{13}C 53.84 ppm; C_6D_6: ^{1}H 7.16 ppm, ^{13}C 128.06 ppm). ^{11}B chemical shifts are reported in ppm relative to the signal of $BF_3{\cdot}OEt_2$ (0.00 ppm). High resolution mass spectrum data were obtained *via* ESI (Agilent (Q-TOF 6520)) analyser. UV/vis spectra were obtained on an Agilent Cary 300 UV/vis spectrophotometer. Fluorescence spectra were recorded on a Photon Technologies International Quanta Master Model C-60 spectrometer. Fluorescent quantum efficiencies were determined using a Hamamatsu Quantaurus-QY spectrometer (C11347). The purity of all compounds reported were established by ^{1}H NMR and ^{13}C NMR spectra.

X-ray crystallographic analyses

The crystal data were collected on a Bruker D8-Venture diffractometer with Mo-target (λ = 0.71073 Å) at 180 K for all compounds except **5a** and **6a** that were collected at 220 K. Data were processed on a PC with the aid of the Bruker SHELXTL software package[25] and corrected for absorption effects. All non-hydrogen atoms were refined anisotropically. The positions of hydrogen atoms were calculated and refined isotropically. The detail of crystal data, collection parameters and results of analyses are provided in the ESI.† The crystal data were deposited to the Cambridge Crystallographic Data Centre with deposition numbers of CCDC 1590110 (**1a**), 1590111 (**3a**), 1590113 (**4a**), 1816881 (**5a**), 1590195 (**6a**), 1590116 (**7a**), 1816882 (**9a**), 1590114 (**1c**), 1590115 (**2c**), 1590112 (**1d**), 1590109 (**2d**), 1811865 (**6d**).‡

DFT calculation details

DFT calculations were performed using the Gaussian 09 suite of programs[26] at the Center for Advanced Computing at Queen's University. Geometry optimizations and vertical excitations of all compounds were obtained at the B3LYP[27]/6-31g(d)[28] level of theory and the resulting structures were confirmed to be stationary points through vibrational frequency analysis. To obtain more accurate energies, subsequent geometry optimizations were performed with M06-2X[29]/6-31g(d), followed by single point energy calculations at the M06-2X/6-31+g(d,p) level of theory with implicit solvent effects (C_6H_6) accounted for using the conducting polarizable continuum model (C-PCM).[30]

Synthesis of compounds *E*-1a–*E*-9a

The ylides reagent (0.42 mmol) was dissolved in THF (10 mL) under argon and cooled to 0 °C. Sodium hydride (0.5 mmol, 60% dispersion in mineral oil) was added in small portions and the solution was stirred for 1 hour. The aromatic aldehyde compound (0.5 mmol) was then added and the reaction was warmed to room temperature and stirred for 12 hours. The solution was concentrated *in vacuo*. The crude product was purified by silica gel chromatography using the appropriate solvents as the eluent.

Data for *E*-1a. Yellow solid (yield: 90%, using 3 : 1 of petroleum ether and ethyl acetate as the eluent). ^{1}H NMR (400 MHz, C_6D_6): δ 8.47 (d, J = 4.6 Hz, 1H), 7.93 (d, J = 16.3 Hz, 1H), 7.60 (d, J = 8.5 Hz, 1H), 7.45 (d, J = 16.3 Hz, 1H), 7.10–7.04 (m, 2H), 6.78 (d, J = 8.5 Hz, 5H), 6.60–6.53 (m, 1H), 6.35 (d, J = 8.4 Hz, 1H), 2.36 (s, 6H), 2.28 (s, 12H), 2.17 (s, 6H). ^{13}C NMR (101 MHz, CD_2Cl_2): δ 157.45, 153.25, 149.31, 145.00, 140.63, 139.86, 138.58, 136.03, 135.59, 134.65, 129.03, 128.57, 121.71, 120.12, 111.31, 108.55, 40.19, 23.24, 21.24. ^{11}B NMR (128 MHz, C_6D_6): δ 70.5. HR-ESIMS (m/z): $[M + H]^+$ calcd for $C_{33}H_{38}BN_2$, 473.3123; found 473.3122.

Data for *E*-2a. Yellow solid (yield: 95%, using 3 : 1 of petroleum ether and ethyl acetate as the eluent). ^{1}H NMR (400 MHz, C_6D_6): δ 8.02 (d, J = 16.2 Hz, 1H), 7.60 (d, J = 8.5 Hz, 1H), 7.37 (d, J = 16.2 Hz, 1H), 7.07 (dd, J = 8.5, 5.1 Hz, 2H), 6.81 (s, 4H), 6.66 (d, J = 7.9 Hz, 1H), 6.54 (d, J = 7.5 Hz, 1H), 6.36 (dd, J = 8.5, 2.5 Hz, 1H), 2.41 (s, 3H), 2.39 (s, 6H), 2.29 (s, 12H), 2.18 (s, 6H). ^{13}C NMR (101 MHz, CD_2Cl_2): δ 157.94, 156.59, 153.21, 144.96, 144.50, 140.69, 139.63, 138.51, 136.32, 135.24, 134.95, 128.97, 128.56, 121.16, 117.47, 111.27, 108.35, 40.21, 24.47, 23.23, 21.24. ^{11}B NMR (225 MHz, C_6D_6): δ 70.1. HR-ESIMS (m/z): $[M + H]^+$ calcd for $C_{34}H_{40}BN_2$, 487.3279; found 487.3289.

Data for *E*-3a. Yellow green solid (yield: 95%, using 2 : 1 of petroleum ether and CH_2Cl_2 as the eluent). ^{1}H NMR (400 MHz, C_6D_6): δ 7.75 (s, 2H), 7.61 (d, J = 8.5 Hz, 1H), 7.18 (d, J = 2.5 Hz, 1H), 7.07–7.02 (m, 1H), 6.94 (dd, J = 7.8, 1.6 Hz, 1H), 6.87 (d, J = 7.7 Hz, 1H), 6.83 (d, J = 7.4 Hz, 4H), 6.49 (d, J = 8.2 Hz, 1H), 6.37 (dd, J = 8.5, 2.6 Hz, 1H), 3.30 (s, 3H), 2.41 (s, 6H), 2.29 (s, 12H), 2.21 (s, 6H). ^{13}C NMR (101 MHz, CD_2Cl_2): δ 156.93, 153.23, 146.17, 144.66, 140.69, 139.67, 138.51, 134.67, 131.48, 128.49, 127.30, 126.68, 122.62, 120.72, 110.94, 110.77, 108.01, 55.81, 40.21, 23.22, 21.27. ^{11}B NMR (225 MHz, C_6D_6): δ 70.4. HR-ESIMS (m/z): $[M + H]^+$ calcd for $C_{35}H_{41}BNO$, 502.3276; found 502.3288.

Data for *E*-4a. Pale yellow solid (yield: 65%, using 5 : 1 of petroleum ether and CH_2Cl_2 as the eluent). ^{1}H NMR (400 MHz, C_6D_6): δ 7.72 (d, J = 16.1 Hz, 1H), 7.62 (d, J = 8.5 Hz, 1H), 7.11 (d, J = 7.4 Hz, 2H), 7.03 (dd, J = 14.7, 9.3 Hz, 5H), 6.82 (s, 4H), 6.39 (dd, J = 8.5, 2.4 Hz, 1H), 2.47 (s, 6H), 2.29 (s, 12H), 2.19 (s, 6H). ^{13}C NMR (101 MHz, CD_2Cl_2): δ 153.21, 145.60, 144.65, 140.62, 139.86, 138.61, 138.44, 131.50, 128.60, 128.17, 127.37, 126.83, 110.97, 107.89, 40.22, 23.24, 21.27. ^{11}B NMR (128 MHz, CD_2Cl_2):

δ 72.4. HR-ESIMS (m/z): $[M + H]^+$ calcd for $C_{34}H_{39}BN$, 472.3170; found 472.3163.

Data for *E*-4a′. Pale yellow solid (yield: 66%, using 5 : 1 of petroleum ether and CH_2Cl_2 as the eluent). ^{1}H NMR (400 MHz, C_6D_6): δ 7.73 (d, J = 16.1 Hz, 1H), 7.63 (d, J = 8.5 Hz, 1H), 7.02 (d, J = 15.7 Hz, 2H), 6.82 (s, 4H), 6.39 (d, J = 8.5 Hz, 1H), 2.46 (s, 6H), 2.29 (s, 12H), 2.19 (s, 6H). ^{13}C NMR (176 MHz, CD_2Cl_2): δ 152.68, 145.17, 144.18, 140.16, 139.42, 138.17, 137.83, 134.17, 130.99, 128.14, 127.80, 127.72, 127.67, 127.53, 126.59, 126.45, 126.31, 126.12, 125.98, 125.85, 110.61, 107.52, 39.88, 22.82, 20.85. ^{11}B NMR (225 MHz, CD_2Cl_2): δ 71.3. HR-ESIMS (m/z): $[M + H]^+$ calcd for $C_{34}H_{34}D_5BN$, 477.3484; found 477.3490.

Data for *E*-5a. White solid (yield: 43%, using 10 : 1 petroleum ether and ethyl acetate as the eluent). ^{1}H NMR (400 MHz, CD_2Cl_2) δ 8.43 (ddd, J = 4.8, 1.7, 0.8 Hz, 1H), 7.75 (d, J = 7.8 Hz, 1H), 7.53–7.41 (m, 3H), 7.33–7.23 (m, 2H), 7.03 (ddd, J = 7.4, 4.9, 0.9 Hz, 1H), 6.93 (d, J = 16.3 Hz, 1H), 6.85–6.76 (m, 5H), 2.25 (s, 6H), 2.01 (s, 12H). ^{13}C NMR (176 MHz, $CDCl_3$) δ 156.22, 147.81, 147.50, 143.55, 141.09, 140.59, 139.37, 137.25, 135.76, 131.64, 128.64, 128.50, 127.36, 125.63, 121.84, 120.27, 23.30, 21.34. ^{11}B NMR (225 MHz, C_6D_6) δ 74.68. HR-ESIMS (m/z): $[M + H]^+$ calcd for $C_{31}H_{33}BN$, 430.2701; found 430.2707.

Data for *E*-6a. Yellow solid (yield: 98%, using 10 : 1 of petroleum ether and CH_2Cl_2 as the eluent). ^{1}H NMR (400 MHz, C_6D_6): δ 7.61 (d, J = 8.5 Hz, 1H), 7.53 (d, J = 16.1 Hz, 1H), 6.99 (dd, J = 9.2, 6.8 Hz, 2H), 6.87–6.76 (m, 5H), 6.72 (t, J = 3.8 Hz, 2H), 6.38 (dd, J = 8.5, 2.4 Hz, 1H), 2.47 (s, 6H), 2.28 (s, 12H), 2.19 (s, 6H). ^{13}C NMR (101 MHz, CD_2Cl_2): δ 153.18, 145.59, 144.53, 141.23, 140.59, 139.84, 138.56, 128.54, 125.71, 125.63, 122.39, 121.80, 110.86, 107.52, 53, 40.20, 23.23, 21.26. ^{11}B NMR (225 MHz, C_6D_6): δ 70.9. HR-ESIMS (m/z): $[M + H]^+$ calcd for $C_{32}H_{37}BNS$, 478.2734; found 478.2751.

Data for *E*-7a. Yellow solid (yield: 88%, using 10 : 1 of petroleum ether and CH_2Cl_2 as the eluent). ^{1}H NMR (400 MHz, C_6D_6): δ 7.59 (d, J = 1.6 Hz, 1H), 7.56 (d, J = 5.6 Hz, 1H), 7.11 (d, J = 15.9 Hz, 1H), 6.93 (d, J = 2.4 Hz, 1H), 6.84 (s, 4H), 6.67 (ddd, J = 8.5, 7.6, 4.3 Hz, 3H), 6.37 (dd, J = 8.5, 2.5 Hz, 1H), 2.44 (s, 6H), 2.30 (s, 12H), 2.20 (s, 6H). ^{13}C NMR (101 MHz, CD_2Cl_2): δ 153.06, 144.98, 144.33, 143.93, 140.59, 139.40, 138.56, 134.96, 130.86, 128.61, 127.57, 125.50, 124.60, 121.36, 111.02, 107.67, 40.24, 23.22, 21.28. ^{11}B NMR (225 MHz, C_6D_6): δ 69.06. HR-ESIMS (m/z): $[M + H]^+$ calcd for $C_{32}H_{37}BNS$, 478.2734; found 478.2742.

Data for *E*-8a. Yellow solid (yield: 85%, using CH_2Cl_2 as the eluent). ^{1}H NMR (400 MHz, C_6D_6) δ 8.45 (d, J = 15.8 Hz, 2H), 8.31 (s, 1H), 7.70 (d, J = 8.1 Hz, 1H), 7.07 (d, J = 15.9 Hz, 1H), 6.91 (t, J = 7.6 Hz, 1H), 6.84 (s, 4H), 6.77 (d, J = 8.1 Hz, 1H), 6.54–6.48 (m, 1H), 6.44 (d, J = 7.8 Hz, 1H), 2.52 (s, 6H), 2.26 (s, 12H), 2.21 (s, 6H). ^{13}C NMR (101 MHz, C_6D_6) δ 156.69, 156.50, 149.89, 141.12, 138.86, 138.49, 137.71, 135.88, 132.26, 129.39, 128.91, 127.34, 122.49, 121.49, 117.30, 43.78, 23.94, 21.34. ^{11}B NMR (225 MHz, C_6D_6) δ 73.93. HR-ESIMS (m/z): $[M + H]^+$ calcd for $C_{33}H_{38}BN_2$, 473.3123; found 473.3120.

Data for *E*-9a. Orange-yellow solid (yield: 51%, using 10 : 1 petroleum ether and ethyl acetate as the eluent). ^{1}H NMR (400 MHz, C_6D_6) δ 8.07 (d, J = 15.9 Hz, 1H), 7.83 (d, J = 8.7 Hz, 1H), 7.21 (d, J = 16.1 Hz, 1H), 7.04 (t, J = 7.7 Hz, 1H), 6.95 (s, 1H), 6.78 (s, 4H), 6.68 (d, J = 7.8 Hz, 1H), 6.63 (d, J = 8.6 Hz, 1H), 6.50 (d, J = 7.5 Hz, 1H), 2.41 (s, 3H), 2.39 (s, 6H), 2.27 (s, 12H), 2.13 (s, 6H). ^{13}C NMR (101 MHz, C_6D_6) δ 157.92, 157.23, 150.18, 144.38, 140.86, 139.07, 135.85, 133.93, 130.58, 129.06, 126.60, 126.00, 120.14, 118.13, 117.56, 115.45, 39.81, 24.60, 23.53, 21.31. ^{11}B NMR (225 MHz, C_6D_6) δ 76.01. HR-ESIMS (m/z): $[M + H]^+$ calcd for $C_{34}H_{40}BN_2$, 487.3279; found 487.3274.

Photoisomerisation of *E*-1a–*E*-9a

NMR scale reactions. In a N_2 filled glovebox, 1 mg of the stilbene (***E*-1a–*E*-9a**) was dissolved in C_6D_6 (0.6 mL) and placed inside a quartz J-Young NMR tube, which was tightly sealed with the Teflon cap and removed from the glovebox. Photoisomerisation experiments were performed in a Shanghaisile Photochemical Reactor (365 nm, internal temperature = r.t. to ~70 °C). The reaction was monitored periodically by ^{1}H NMR spectra until no spectral change was observed. The conversion of ***E*-1a–*E*-4a** to **1b–4b** is quantitative. Compounds **1b–4b** can be isolated as air-stable light-yellow solids by simply removing the solvent under vacuum.

Preparative scale reactions

To an oven-dried Schlenk flask was added the stilbene compound (***E*-1a–*E*-4a**, ~0.01 mmol). The flask was evacuated and filled with N_2 three times. Freshly distilled benzene (4 mL) was injected into the Schlenk flask under nitrogen. The solution was then irradiated with 365 nm UV light at room temperature for 2–7 h until the starting material stilbene was completely consumed according to TLC. After removing the solvent under reduced pressure, compounds **1b–4b** were obtained quantitatively as pure products and confirmed by NMR spectroscopy. Compounds **1b–4b** cannot be further purified by column chromatography. Compound ***E*-6a** partially converts to **6b** under 365 nm irradiation, which could not be isolated as a pure compound from the reaction mixture (see Fig. S20–S22 in the ESI†). Compounds ***E*-7a–*E*-9a** only undergoes photoisomerisation to ***Z*-7a–*Z*-9a** (see Fig. S24–S27 in the ESI†). The characterization data provided below are for isolated compounds **1b–4b**.

Data for 1b. Yellow brown solid. ^{1}H NMR (400 MHz, C_6D_6): δ 8.41 (d, J = 4.5 Hz, 1H), 8.06 (d, J = 7.8 Hz, 1H), 6.94–6.68 (m, 7H), 6.66 (dd, J = 7.8, 4.8 Hz, 1H), 4.98 (d, J = 6.9 Hz, 1H), 3.86 (d, J = 20.6 Hz, 1H), 3.66 (d, J = 20.8 Hz, 1H), 2.54 (s, 6H), 2.18 (s, 12H), 1.85 (s, 6H). ^{13}C NMR (176 MHz, C_6D_6): δ 155.25, 155.21, 147.52, 145.65, 143.01, 141.39, 139.25, 138.02, 137.83, 134.65, 131.05, 128.92, 128.81, 120.55, 101.86, 43.20, 41.49, 39.87, 21.28. ^{11}B NMR (225 MHz, C_6D_6): δ 68.4. HR-ESIMS (m/z): $[M + H]^+$ calcd for $C_{33}H_{38}BN_2$, 473.3123; found 473.3121.

Data for 2b. Yellow brown solid. ^{1}H NMR (400 MHz, C_6D_6): δ 8.03 (d, J = 8.0 Hz, 1H), 6.94–6.68 (m, 7H), 6.66 (d, J = 8.0 Hz, 1H), 4.99 (d, J = 6.9 Hz, 1H), 3.87 (d, J = 22.8 Hz, 1H), 3.68 (d, J = 20.6 Hz, 1H), 2.62 (s, 6H), 2.42 (s, 3H), 2.18 (s, 12H), 1.92 (s, 6H). ^{13}C NMR (176 MHz, C_6D_6): δ 155.77, 155.52, 154.54, 145.69, 142.86, 141.34, 139.21, 138.16, 137.78, 131.83, 131.54, 128.98, 128.79, 119.80, 101.75, 43.50, 41.37, 39.92, 24.11, 21.28. ^{11}B NMR (225 MHz, C_6D_6): δ 68.0. HR-ESIMS (m/z): $[M + H]^+$ calcd for $C_{34}H_{40}BN_2$, 487.3279; found 487.3289.

Data for 3b. Yellow solid. ^{1}H NMR (400 MHz, C_6D_6): δ 7.72 (d, J = 7.8 Hz, 1H), 7.09–7.02 (m, 2H), 6.95 (d, J = 6.8 Hz, 1H), 6.77 (s, 2H), 6.69 (d, J = 9.6 Hz, 1H), 6.62 (s, 2H), 6.44 (d, J = 8.2 Hz, 1H), 5.03 (d, J = 6.9 Hz, 1H), 3.90 (d, J = 20.3 Hz, 1H), 3.72 (d, J = 20.6 Hz, 1H), 3.17 (s, 3H), 2.70 (s, 3H), 2.37 (s, 3H), 2.19 (s, 12H), 2.05 (s, 6H). ^{13}C NMR (176 MHz, C_6D_6): δ 156.13, 155.24, 146.26, 141.68, 139.24, 137.43, 132.22, 128.77, 126.76, 124.93, 121.34, 118.38, 117.04, 109.90, 108.93, 101.10, 93.72, 54.81, 42.86, 40.49, 39.58, 21.29. ^{11}B NMR (225 MHz, C_6D_6): δ 65.9. HR-ESIMS (m/z): $[M + H]^+$ calcd for $C_{35}H_{41}BNO$, 502.3276; found 502.3287.

Data for 4b. Yellow solid. ^{1}H NMR (400 MHz, C_6D_6): δ 8.00 (d, J = 7.5 Hz, 1H), 7.10–7.00 (m, 2H), 6.95–6.91 (m, 1H), 6.84 (d, J = 7.3 Hz, 1H), 6.86–6.67 (m, 4H), 6.64 (dd, J = 9.3, 2.4 Hz, 1H), 6.24 (dd, J = 9.3, 2.6 Hz, 1H), 5.02 (d, J = 6.9 Hz, 1H), 3.86 (d, J = 20.4 Hz, 1H), 3.71 (d, J = 20.5 Hz, 1H), 2.68 (s, 3H), 2.38 (s, 3H), 2.19 (s, 12H), 1.99 (s, 6H). ^{13}C NMR (176 MHz, C_6D_6): δ 156.17, 146.38, 141.47, 139.84, 139.81, 139.33, 137.54, 136.10, 128.77, 127.67, 126.80, 126.66, 126.23, 126.08, 124.44, 101.24, 43.29, 42.36, 39.97, 21.29. ^{11}B NMR (225 MHz, C_6D_6): δ 67.4. HR-ESIMS (m/z): $[M + H]^+$ calcd for $C_{34}H_{39}BN$, 472.3170; found 472.3182.

Thermal isomerisation of 1b–4b

NMR scale reactions. 1 mg of the stilbenes (***E*-1a–*E*-4a**) in C_6D_6 (0.6 mL) was converted to the corresponding 4a,4b-DHPs (**1b–4b**) in the same manner as described in the photoisomerisation section. After full conversion, the NMR tubes were heated in an oil bath to the appropriate temperature to convert **1b–4b** to their isomers **1c–4c**. The thermal isomerisation was monitored by NMR spectroscopy. After compounds **1b–4b** were fully converted to **1c–4c**, removal of the solvent in vacuum led to the quantitative isolation of pure **1c–4c**.

Preparative scale reactions

To an oven-dried Schlenk flask was added the stilbene compound (***E*-1a–*E*-4a**, ~0.03 mmol), which was converted to the corresponding 4a,4b-DHP (**1b–4b**) in the same manner as described in the photoisomerisation reaction. After the full conversion, the solution was heated at 120 °C for 24 h (**1b**, **2b**), 8 h (**3b**), 24 h (**4b**). After being cooled to room temperature, the solvents were then removed under reduced pressure and compounds **1c–4c** were obtained nearly quantitatively. These four compounds can be further purified by either column chromatography using petroleum ether and ethyl acetate as the eluent or recrystallization by the slow evaporation of the solvent (benzene or CH_2Cl_2) under air.

Data for 1c. Yellow solid. ^{1}H NMR (700 MHz, C_6D_6): δ 8.46 (d, J = 4.6 Hz, 1H), 6.91 (s, 1H), 6.89–6.85 (m, 2H), 6.77 (d, J = 7.5 Hz, 2H), 6.72–6.68 (m, 2H), 6.67 (dd, J = 7.6, 4.9 Hz, 1H), 5.97 (dd, J = 9.8, 7.0 Hz, 1H), 4.68 (d, J = 6.5 Hz, 1H), 3.54 (d, J = 7.5 Hz, 1H), 3.48 (td, J = 7.3, 2.5 Hz, 1H), 2.54 (s, 3H), 2.24 (s, 3H), 2.22 (s, 3H), 2.21 (s, 3H), 2.16 (s, 6H), 2.14 (s, 3H), 1.84 (s, 3H). ^{13}C NMR (101 MHz, C_6D_6): δ 155.32, 154.23, 148.81, 148.03, 142.20, 141.06, 139.91, 138.82, 137.95, 137.42, 137.30, 132.33, 130.95, 128.92, 128.73, 121.52, 93.62, 39.79, 39.26, 38.39, 24.07, 22.71, 22.64, 22.12, 21.35, 21.32. ^{11}B NMR (128 MHz, C_6D_6): δ 69.0. HR-ESIMS (m/z): $[M + H]^+$ calcd for $C_{33}H_{38}BN_2$, 473.3123; found 473.3125.

Data for 2c. Yellow solid. ^{1}H NMR (400 MHz, C_6D_6): δ 6.91 (s, 1H), 6.90–6.84 (m, 2H), 6.78 (s, 1H), 6.75 (s, 1H), 6.72–6.67 (m, 3H), 5.99 (dd, J = 9.8, 6.9 Hz, 1H), 4.70 (d, J = 6.5 Hz, 1H), 3.57 (d, J = 7.4 Hz, 1H), 3.51 (td, J = 7.2, 2.4 Hz, 1H), 2.55 (s, 3H), 2.50 (s, 3H), 2.26–2.20 (m, 9H), 2.19 (s, 6H), 2.14 (s, 3H), 1.89 (s, 3H). ^{13}C NMR (176 MHz, C_6D_6): δ 156.44, 154.61, 154.49, 148.70, 145.07, 143.59, 142.27, 141.09, 139.90, 138.84, 137.66, 137.56, 137.38, 137.25, 132.81, 128.89, 128.70, 128.59, 128.31, 127.68, 127.60, 120.68, 93.52, 39.55, 39.41, 38.43, 24.27, 24.09, 22.72, 22.69, 22.12, 21.35, 21.25. ^{11}B NMR (225 MHz, C_6D_6): δ 67.7. HR-ESIMS (m/z): $[M + H]^+$ calcd for $C_{34}H_{40}BN_2$, 487.3279; found 487.3281.

Data for 3c. Yellow solid. ^{1}H NMR (400 MHz, C_6D_6): δ 7.05 (t, J = 8.0 Hz, 1H), 6.93 (t, J = 10.2 Hz, 3H), 6.80 (s, 2H), 6.70 (s, 1H), 6.54 (t, J = 8.1 Hz, 2H), 5.82 (dd, J = 9.7, 6.8 Hz, 1H), 4.78 (d, J = 6.5 Hz, 1H), 3.59 (d, J = 7.3 Hz, 1H), 3.57–3.52 (m, 1H), 3.37 (s, 3H), 2.59 (s, 3H), 2.27 (d, J = 5.2 Hz, 9H), 2.24 (d, J = 4.1 Hz, 6H), 2.15 (s, 3H), 1.89 (s, 3H). ^{13}C NMR (176 MHz, C_6D_6): δ 156.06, 155.03, 149.27, 145.54, 143.88, 142.78, 141.05, 139.01, 137.77, 137.10, 136.97, 136.56, 132.22, 128.73, 128.65, 128.59, 128.31, 127.48, 125.10, 119.32, 118.38, 109.90, 93.72, 55.45, 40.49, 39.30, 38.51, 23.97, 22.76, 22.69, 22.22, 21.38, 21.26. ^{11}B NMR (225 MHz, C_6D_6): δ 66.9. HR-ESIMS (m/z): $[M + H]^+$ calcd for $C_{35}H_{41}BNO$, 502.3276; found 502.3286.

Data for 4c. Yellow solid. ^{1}H NMR (400 MHz, C_6D_6): δ 7.12–7.03 (m, 2H), 6.93 (d, J = 4.0 Hz, 2H), 6.89 (d, J = 7.0 Hz, 1H), 6.81 (d, J = 6.9 Hz, 2H), 6.78 (s, 1H), 6.70 (s, 1H), 6.19 (d, J = 9.6 Hz, 1H), 5.78 (dd, J = 9.4, 6.8 Hz, 1H), 4.76 (d, J = 6.5 Hz, 1H), 3.61–3.52 (m, 2H), 2.58 (s, 3H), 2.27 (s, 3H), 2.25 (s, 6H), 2.22 (d, J = 2.4 Hz, 6H), 2.15 (s, 3H), 1.83 (s, 3H). ^{13}C NMR (176 MHz, C_6D_6): δ 155.84, 149.45, 145.51, 143.77, 142.46, 141.03, 139.69, 139.10, 137.37, 137.18, 137.01, 136.00, 135.18, 133.48, 128.70, 128.67, 128.60, 128.31, 127.29, 127.08, 125.75, 125.54, 125.13, 93.60, 40.28, 39.62, 38.45, 24.00, 22.76, 22.73, 22.19, 21.38, 21.25. ^{11}B NMR (225 MHz, C_6D_6): δ 66.8. HR-ESIMS (m/z): $[M + H]^+$ calcd for $C_{34}H_{39}BN$, 472.3170; found 472.3183.

Synthesis of compounds 1d–4d and 6d

To a Schlenk flask was added the stilbene compound (***E*-1a–*E*-4a** and ***E*-6a**, ~0.04 mmol), and THF (40 mL) under the air. The Schlenk flask was then closed and irradiated with 365 nm UV light at room temperature for 2 h. The solution was concentrated *in vacuo*. The crude product was purified by silica gel chromatography using appropriate solvents as the eluents.

Data for 1d. Pale yellow solid (yield: 32%, using CH_2Cl_2 as the eluent). ^{1}H NMR (400 MHz, C_6D_6): δ 9.92 (d, J = 8.7 Hz, 1H), 8.82 (d, J = 4.1 Hz, 1H), 8.51 (d, J = 9.2 Hz, 1H), 8.02 (d, J = 9.2 Hz, 1H), 7.70 (d, J = 7.9 Hz, 1H), 7.02 (dd, J = 8.7, 4.1 Hz, 1H), 6.91 (d, J = 7.9 Hz, 1H), 6.79 (s, 4H), 2.35 (s, 6H), 2.17 (s, 12H), 2.15 (s, 6H). ^{13}C NMR (176 MHz, C_6D_6): δ 155.79, 149.18, 149.03, 144.42, 142.97, 140.86, 139.17, 138.64, 136.41, 134.10, 134.04, 131.12, 129.89, 129.13, 126.68, 122.56, 120.27, 115.61, 43.60, 23.42, 21.34. ^{11}B NMR (225 MHz, C_6D_6): δ 73.7. HR-ESIMS (m/z): $[M + H]^+$ calcd for $C_{33}H_{36}BN_2$, 471.2966; found 471.2980.

Data for 2d. Pale yellow solid (yield: 32%, using CH_2Cl_2 as the eluent). ^{1}H NMR (400 MHz, C_6D_6): δ 9.91 (d, J = 8.8 Hz, 1H), 8.53 (d, J = 9.2 Hz, 1H), 8.04 (d, J = 9.2 Hz, 1H), 7.69 (d, J = 7.9 Hz, 1H), 7.03 (d, J = 8.8 Hz, 1H), 6.93 (d, J = 8.0 Hz, 1H), 6.78 (s, 4H), 2.60 (s, 3H), 2.41 (s, 6H), 2.17 (s, 18H). ^{13}C NMR (176 MHz, C_6D_6): δ 157.56, 155.63, 148.65, 144.38, 143.10, 140.82, 139.35, 136.05, 134.56, 134.50, 131.08, 129.55, 129.11, 124.56, 122.83, 120.64, 115.56, 43.67, 24.82, 23.37, 21.34. ^{11}B NMR (225 MHz, C_6D_6): δ 74.0. HR-ESIMS (m/z): $[M + H]^+$ calcd for $C_{34}H_{38}BN_2$, 485.3123; found 485.3124.

Data for 3d. Pale yellow solid (yield: 37%, using 5 : 1 of petroleum ether and CH_2Cl_2 as the eluent). ^{1}H NMR (400 MHz, C_6D_6): δ 9.56 (d, J = 8.8 Hz, 1H), 8.36 (d, J = 9.3 Hz, 1H), 8.29 (d, J = 9.3 Hz, 1H), 7.72 (d, J = 7.9 Hz, 1H), 7.41 (t, J = 8.2 Hz, 1H), 6.93 (d, J = 7.9 Hz, 1H), 6.79 (s, 4H), 6.63 (d, J = 7.7 Hz, 1H), 3.40 (s, 3H), 2.50 (s, 6H), 2.19 (s, 12H), 2.16 (s, 6H). ^{13}C NMR (176 MHz, C_6D_6): δ 155.89, 155.78, 144.64, 142.30, 140.86, 139.49, 138.80, 136.36, 132.79, 129.04, 126.94, 125.64, 124.43, 122.88, 121.38, 119.64, 114.87, 105.32, 55.20, 43.82, 23.47, 21.36. ^{11}B NMR (225 MHz, C_6D_6): δ 72.9. HR-ESIMS (m/z): $[M + H]^+$ calcd for $C_{35}H_{39}BNO$, 500.3119; found 500.3144.

Data for 4d. Pale yellow solid (yield: 37%, using 5 : 1 of petroleum ether and CH_2Cl_2 as the eluent). ^{1}H NMR (400 MHz, C_6D_6): δ 9.88 (d, J = 8.7 Hz, 1H), 8.30 (d, J = 9.0 Hz, 1H), 7.70 (d, J = 7.9 Hz, 1H), 7.54 (d, J = 7.9 Hz, 1H), 7.46 (t, J = 7.7 Hz, 1H), 7.33 (t, J = 7.4 Hz, 1H), 7.26 (d, J = 9.0 Hz, 1H), 6.93 (d, J = 7.9 Hz, 1H), 6.81 (s, 4H), 2.46 (s, 6H), 2.19 (s, 12H), 2.18 (s, 6H). ^{13}C NMR (176 MHz, C_6D_6): δ 155.75, 144.63, 142.54, 140.86, 139.20, 138.90, 136.18, 132.98, 131.66, 129.07, 128.43, 127.58, 127.17, 127.11, 126.00, 125.80, 122.99, 115.01, 43.76, 23.49, 21.37. ^{11}B NMR (225 MHz, C_6D_6): δ 73.6. HR-ESIMS (m/z): $[M + H]^+$ calcd for $C_{34}H_{37}BN$, 470.3014; found 470.3036.

Data for 6d. Pale yellow solid (yield: 37%, using 10 : 1 of petroleum ether and CH_2Cl_2 as the eluent). ^{1}H NMR (400 MHz, C_6D_6): δ 8.26 (d, J = 8.8 Hz, 1H), 7.68 (d, J = 7.6 Hz, 1H), 7.45 (d, J = 8.8 Hz, 1H), 7.22 (s, 1H), 7.11–7.05 (m, 2H), 6.80 (s, 4H), 2.55 (s, 6H), 2.18 (s, 12H), 2.16 (s, 6H). ^{13}C NMR (176 MHz, C_6D_6): δ 153.95, 145.52, 144.43, 140.89, 139.17, 138.53, 136.30, 134.41, 134.38, 129.10, 128.53, 127.01, 125.36, 123.67, 123.35, 117.44, 45.17, 23.49, 21.35. ^{11}B NMR (225 MHz, C_6D_6): δ 75.0. HR-ESIMS (m/z): $[M + H]^+$ calcd for $C_{32}H_{35}BNS$, 476.2578; found 476.2601.

Conflicts of interest

There are no conflicts to declare.

Acknowledgements

Y. G. Shi, G. F. Hu, T. Peng, N. Wang, P. Chen and S. Wang thank the National Natural Science Foundation of China for financial support (grant no. 21701011, 21501011, 21772012, 21571017) for financial support. S. K. Mellerup, K. Yuan and S. Wang thank the Natural Sciences and Engineering Research Council of Canada (RGPIN1193993-2013) for financial support and the Centre for Advanced Computing at Queen's University for computational facilities. S. K. Mellerup thanks the Canadian government for the Vanier CGS.

Notes and references

1 For select examples see: (*a*) R. G. W. Norrish and C. H. Bamford, *Nature*, 1937, **140**, 195; (*b*) H. E. Zimmerman and A. C. Pratt, *J. Am. Chem. Soc.*, 1970, **92**, 6259; (*c*) Y. Inoue, *Chem. Rev.*, 1992, **92**, 741 and references therein; (*d*) G. S. Hammond, J. Saltiel, A. A. Lamola, N. J. Turro, J. S. Bradshaw, D. O. Cowan, R. C. Counsell, V. Vogt and C. Dalton, *J. Am. Chem. Soc.*, 1964, **86**, 3197.

2 (*a*) F. R. Stermitz, *Org. Photochem.*, 1967, **1**, 247; (*b*) M. Scholz, F. Dietz and Z. Mühlstädt, *Chem*, 1967, **7**, 329; (*c*) *Preparative Organic Photochemistry*, ed. A. Schönberg, Springer-Verlag, New York, 1968; (*d*) S. T. Reid, *Adv. Heterocycl. Chem.*, 1970, **23**, 87; (*e*) J. Grimshaw and A. P. de Silva, *Chem. Soc. Rev.*, 1981, **10**, 181; (*f*) F. B. Mallory, C. S. Wood and J. T. Gordon, *J. Am. Chem. Soc.*, 1964, **86**, 3094; (*g*) D. H. Waldeck, *Chem. Rev.*, 1991, **91**, 415; (*h*) W. H. Laarhoven, *Pure Appl. Chem.*, 1984, **56**, 1225; (*i*) H. Meier, *Angew. Chem., Int. Ed.*, 1992, **31**, 1399; (*j*) M. Irie, *Chem. Rev.*, 2000, **100**, 1685; (*k*) W. M. Kwok, C. Ma, D. Philips, A. Beeby, T. B. Marder, R. Ll. Thomas, C. Tschuschke, G. Baranovic, P. Matousek, M. Towrie and A. W. Parker, *J. Raman Spectrosc.*, 2003, **34**, 886.

3 R. B. Woodward and R. Hoffmann, *J. Am. Chem. Soc.*, 1965, **87**, 395.

4 (*a*) F. B. Mallory and C. W. Mallory, *Org. React.*, 2005, **30**, 1; (*b*) J. H. Ho, T. I. Ho and R. S. H. Liu, *Org. Lett.*, 2001, **3**, 409; (*c*) T. I. Ho, J. Y. Wu and S. L. Wang, *Angew. Chem., Int. Ed.*, 1999, **38**, 2558; (*d*) E. N. Gulakova, D. V. Berdnikova, T. M. Aliyeu, Y. V. Fedorov, I. A. Godovikov and O. A. Fedo-rova, *J. Org. Chem.*, 2014, **79**, 5533; (*e*) R. Lapouyade, R. Koussini and J. C. Rayez, *J. Chem. Soc., Chem. Commun.*, 1975, 676; (*f*) F. B. Mallory and C. W. Mallory, *J. Am. Chem. Soc.*, 1972, **94**, 6041; (*g*) J. Han, T. Wang, Y. Liang, Y. Li, C. Li, R. Wang, S. Feng and Z. Zhang, *Org. Lett.*, 2017, **19**, 3552; (*h*) T. M. Aliyeu, D. V. Berdnikova, O. A. Fedorova, E. N. Gulakova, C. Stremmel and H. Ihmels, *J. Org. Chem.*, 2016, **81**, 9075; (*i*) T. Matsushima, S. Kobayashi and S. Watanabe, *J. Org. Chem.*, 2016, **81**, 7799.

5 (*a*) T. D. Doyle, W. R. Benson, D. Banes and N. Filipescu, *J. Am. Chem. Soc.*, 1970, **92**, 6371; (*b*) T. D. Doyle, W. R. Benson and N. Filipescu, *J. Am. Chem. Soc.*, 1976, **98**, 3262.

6 J. B. M. Somers, A. Couture, A. Lablanche-Combier and W. H. Laarhoven, *J. Am. Chem. Soc.*, 1985, **107**, 1387.

7 (*a*) P. Bortolus, G. Cauzzo and G. Galiazzo, *Tetrahedron Lett.*, 1966, 3717; (*b*) P. Bortolus, G. Cauzzo, U. Mazzucato and G. Z. Galiazzo, *Z. Phys. Chem.*, 1969, **63**, 29.

8 (*a*) F. Jäkle, *Chem. Rev.*, 2010, **110**, 3985; (*b*) Y. Ren and F. Jäkle, *Dalton Trans.*, 2016, **45**, 13996; (*c*) Z. M. Hudson and S. Wang, *Acc. Chem. Res.*, 2009, **42**, 1584; (*d*) T. W. Hudnall, C. W. Chiu and F. P. Gabbaï, *Acc. Chem. Res.*, 2009, **42**, 388; (*e*) C. R. Wade, A. E. J. Broomsgrave, S. Aldridge and F. P. Gabbaï, *Chem. Rev.*, 2010, **110**, 3958; (*f*) D. W. Stephan and G. Erker, *Angew. Chem., Int. Ed.*,

2009, **49**, 46; (*g*) E. v. Grotthuss, A. John, T. Kaese and M. Wagner, *Asian J. Org. Chem.*, 2018, **7**, 37; (*h*) L. Ji, S. Griesbeck and T. B. Marder, *Chem. Sci.*, 2017, **8**, 846; (*i*) C. D. Entwistle and T. B. Marder, *Angew. Chem., Int. Ed.*, 2002, **41**, 2927; (*j*) C. D. Entwistle and T. B. Marder, *Chem. Mater.*, 2004, **16**, 4574; (*k*) S. Y. Li, Z. B. Sun and C. H. Zhao, *Inorg. Chem.*, 2017, **56**, 8705.

9 J. M. Janusz, P. A. Young, J. M. Ridgeway, M. W. Scherz, K. Enzweiler, L. I. Wu, L. Gan, J. Chen, D. E. Kellstein and S. A. Green, *J. Med. Chem.*, 1998, **41**, 3515.

10 M. Jeran, A. E. Cotman, M. Stephan and B. Mohar, *Org. Lett.*, 2017, **19**, 2042.

11 J. A. Smith and K. D. Moeller, *Org. Lett.*, 2013, **15**, 5818.

12 Y.-Z. Chen, C.-W. Ni, F.-L. Teng, Y.-S. Ding, T.-H. Lee and J.-H. Ho, *Tetrahedron*, 2014, **70**, 1748.

13 J. N. Ngwendson, W. N. Atemnkeng, C. M. Schultze and A. Banerjee, *Org. Lett.*, 2006, **8**, 4085.

14 Y. G. Shi, J. Wang, H. Li, G. F. Hu, X. Li, S. K. Mellerup, N. Wang, T. Peng and S. Wang, *Chem. Sci.*, 2018, **9**, 1902–1911.

15 (*a*) L. Ji, R. M. Edkins, A. Lorbach, I. Krummenacher, C. Brueckner, A. Eichhorn, H. Braunschweig, B. Engels, P. J. Low and T. B. Marder, *J. Am. Chem. Soc.*, 2015, **137**, 6750; (*b*) C. Reus, S. Weidlich, M. Bolte, H.-W. Lerner and M. Wagner, *J. Am. Chem. Soc.*, 2013, **135**, 12892.

16 A. A. Bothner-By, *Adv. Magn. Opt. Reson.*, 1965, **1**, 195.

17 F. D. Lewis, R. S. Kalgutkar and J. S. Yang, *J. Am. Chem. Soc.*, 2001, **123**, 3878.

18 (*a*) M. V. Sargent and C. J. Timmons, *J. Chem. Soc.*, 1964, 5544; (*b*) R. Lapouyade, A. Veyres, N. Hanafi, A. Couture and A. Lablanche-Combier, *J. Org. Chem.*, 1982, **47**, 1361; (*c*) T. I. Ho, J. H. Ho and J. Y. Wu, *J. Am. Chem. Soc.*, 2000, **122**, 8575.

19 *Modern Physical Organic Chemistry*, ed. E. V. Anslyn and D. A. Dougherty, Wilstead & Taylor Publishing Services, USA, 2005.

20 (*a*) P. Metrangolo, H. Neukirch, T. Pilati and G. Resnati, *Acc. Chem. Res.*, 2005, **38**, 386; (*b*) P. C. Ho, P. Szydlowski, P. J. W. Elder, J. Sinclair, J. Kübel, C. Gendy, L. M. Lee, H. Jenkins, J. F. Britten, D. R. Morim and I. Vargas-Baca, *Nat. Commun.*, 2016, **7**, 11299.

21 (*a*) J. C. Doty, B. Babb, P. J. Grisdale, M. E. Glogowski and J. L. R. Williams, *J. Organomet. Chem.*, 1972, **38**, 229; (*b*) Z. Yuan, C. D. Entwistle, J. C. Collings, D. Albesa-Jov, A. S. Batsanov, J. A. K. Howard, N. J. Taylor, H. M. Kaiser, D. E. Kaufmann, S.-Y. Poon, W.-Y. Wong, C. Jardin, S. Fathallah, A. Boucekkine, J. F. Halet and T. B. Marder, *Chem.–Eur. J.*, 2006, **12**, 2758; (*c*) D. R. Bai, X.-Y. Liu and S. Wang, *Chem.–Eur. J.*, 2007, **13**, 5713; (*d*) Z. Yuan, J. C. Collings, N. J. Taylor, T. B. Marder, C. Jardin and J. F. Halet, *J. Solid State Chem.*, 2000, **154**, 5; (*e*) Z. Zhang, R. M. Edkins, J. Nitsch, K. Fucke, A. Steffen, L. E. Longobardi, D. W. Stephan, C. Lambert and T. B. Marder, *Chem. Sci.*, 2015, **6**, 308; (*f*) Z. Zhang, R. M. Edkins, J. Nitsch, K. Fucke, A. Eichhorn, A. Steffen, Y. Wang and T. B. Marder, *Chem.–Eur. J.*, 2015, **21**, 177.

22 B. Neue, R. Fröhlich, B. Wibbeling, A. Fukazawa, A. Wakamiya, S. Yamaguchi and E.-U. Würthwein, *J. Org. Chem.*, 2012, **77**, 2176.

23 J. Garcia, J. Sorrentino, E. J. Diller, D. Chapman and Z. R. Woydziak, *Synth. Commun.*, 2016, **5**, 475.

24 C. Jimenez, Y. Ellahioui, R. Alvarez, L. Aramburu, A. Riesco, M. Gonzalez, A. Vincente, A. Dahdouh, A. I. Mansour, C. Jimenez, D. Martin, R. G. Sarmiento, M. Medarde, E. Caballero and R. Pelaez, *Eur. J. Med. Chem.*, 2015, **100**, 210.

25 *SHELXTL, version 6.14*, Bruker AXS, Madison, WI, 2000–2003.

26 M. J. Frisch, G. W. Trucks, H. B. Schlegel, G. E. Scuseria, M. A. Robb, J. R. Cheeseman, G. Scalmani, V. Barone, B. Mennucci, G. A. Petersson, H. Nakatsuji, M. Caricato, X. Li, H. P. Hratchian, A. F. Izmaylov, J. Bloino, G. Zheng, J. L. Sonnenberg, M. Hada, M. Ehara, K. Toyota, R. Fukuda, J. Hasegawa, M. Ishida, T. Nakajima, Y. Honda, O. Kitao, H. Nakai, T. Vreven, J. A. Montgomery Jr, J. E. Peralta, F. Ogliaro, M. Bearpark, J. J. Heyd, E. Brothers, K. N. Kudin, V. N. Staroverov, T. Keith, R. Kobayashi, J. Normand, K. Raghavachari, A. Rendell, J. C. Burant, S. S. Iyengar, J. Tomasi, M. Cossi, N. Rega, J. M. Millam, M. Klene, J. E. Knox, J. B. Cross, V. Bakken, C. Adamo, J. Jaramillo, R. Gomperts, R. E. Stratmann, O. Yazyev, A. J. Austin, R. Cammi, C. Pomelli, J. W. Ochterski, R. L. Martin, K. Morokuma, V. G. Zakrzewski, G. A. Voth, P. Salvador, J. J. Dannenberg, S. Dapprich, A. D. Daniels, O. Farkas, J. B. Foresman, J. V. Ortiz, J. Cioslowski and D. J. Fox, *Gaussian 09 Revision C.01*, 2010.

27 (*a*) C. Lee, W. Yang and R. G. Parr, *Phys. Rev. B*, 1988, **37**, 785; (*b*) A. D. Becke, *J. Chem. Phys.*, 1993, **98**, 1372; (*c*) A. D. Becke, *J. Chem. Phys.*, 1993, **98**, 5648.

28 (*a*) R. Ditchfield, W. J. Hehre and J. A. Pople, *J. Chem. Phys.*, 1971, **54**, 724; (*b*) A. D. McLean and G. S. Chandler, *J. Chem. Phys.*, 1980, **72**, 5639.

29 Y. Zhao and D. G. Truhlar, *Theor. Chem. Acc.*, 2008, **120**, 215.

30 (*a*) V. Barone and M. J. Cossi, *J. Phys. Chem. A*, 1998, **102**, 1995; (*b*) R. Cammi, B. Mennucci and J. Tomasi, *J. Phys. Chem. A*, 1999, **103**, 9100; (*c*) J. Tomasi, B. Mennucci and R. Cammi, *Chem. Rev.*, 2005, **105**, 2999.